Eur. Phys. J. C (2016) 76:652
DOI 10.1140/epjc/s10052-016-4454-5

THE EUROPEAN PHYSICAL JOURNAL C

Regular Article - Experimental Physics

Limit on the radiative neutrinoless double electron capture of ^{36}Ar from GERDA Phase I

GERDA Collaboration[1,a]

M. Agostini[1], **M. Allardt**[4], **A. M. Bakalyarov**[13], **M. Balata**[1], **I. Barabanov**[11], **N. Barros**[4,20], **L. Baudis**[19], **C. Bauer**[7], **E. Bellotti**[8,9], **S. Belogurov**[11,12], **S. T. Belyaev**[13], **G. Benato**[19], **A. Bettini**[16,17], **L. Bezrukov**[11], **T. Bode**[15], **D. Borowicz**[3,5], **V. Brudanin**[5], **R. Brugnera**[16,17], **A. Caldwell**[14], **C. Cattadori**[9], **A. Chernogorov**[12], **V. D'Andrea**[1], **E. V. Demidova**[12], **A. di Vacri**[1], **A. Domula**[4], **E. Doroshkevich**[11], **V. Egorov**[5], **R. Falkenstein**[18], **O. Fedorova**[11], **K. Freund**[18], **N. Frodyma**[3], **A. Gangapshev**[7,11], **A. Garfagnini**[16,17], **C. Gooch**[14], **P. Grabmayr**[18], **V. Gurentsov**[11], **K. Gusev**[5,13,15], **J. Hakenmüller**[7], **A. Hegai**[18], **M. Heisel**[7], **S. Hemmer**[17], **G. Heusser**[7], **W. Hofmann**[7], **M. Hult**[6], **L. V. Inzhechik**[11,21], **J. Janicskó Csáthy**[15], **J. Jochum**[18], **M. Junker**[1], **V. Kazalov**[11], **T. Kihm**[7], **I. V. Kirpichnikov**[12], **A. Kirsch**[7], **A. Kish**[19], **A. Klimenko**[5,7,22], **R. Kneißl**[14], **K. T. Knöpfle**[7], **O. Kochetov**[5], **V. N. Kornoukhov**[11,12], **V. V. Kuzminov**[11], **M. Laubenstein**[1], **A. Lazzaro**[15], **V. I. Lebedev**[13], **B. Lehnert**[4], **H. Y. Liao**[14], **M. Lindner**[7], **I. Lippi**[17], **A. Lubashevskiy**[5,7], **B. Lubsandorzhiev**[11], **G. Lutter**[6], **C. Macolino**[1,23], **B. Majorovits**[14], **W. Maneschg**[7], **E. Medinaceli**[16,17], **M. Miloradovic**[19], **R. Mingazheva**[19], **M. Misiaszek**[3], **P. Moseev**[11], **I. Nemchenok**[5], **D. Palioselitis**[14], **K. Panas**[3], **L. Pandola**[2], **K. Pelczar**[3], **A. Pullia**[10], **S. Riboldi**[10], **N. Rumyantseva**[5], **C. Sada**[16,17], **F. Salamida**[9], **M. Salathe**[7], **C. Schmitt**[18], **B. Schneider**[4], **S. Schönert**[15], **J. Schreiner**[7], **A.-K. Schütz**[18], **O. Schulz**[14], **B. Schwingenheuer**[7], **O. Selivanenko**[11], **M. Shirchenko**[5,13], **H. Simgen**[7], **A. Smolnikov**[7], **L. Stanco**[17], **M. Stepaniuk**[7], **L. Vanhoefer**[14], **A. A. Vasenko**[12], **A. Veresnikova**[11], **K. von Sturm**[16,17], **V. Wagner**[7], **M. Walter**[19], **A. Wegmann**[7], **T. Wester**[4], **C. Wiesinger**[15], **H. Wilsenach**[4], **M. Wojcik**[3], **E. Yanovich**[11], **I. Zhitnikov**[5], **S. V. Zhukov**[13], **D. Zinatulina**[5], **K. Zuber**[4], **G. Zuzel**[3]

[1] INFN Laboratori Nazionali del Gran Sasso and Gran Sasso Science Institute, Assergi, Italy
[2] INFN Laboratori Nazionali del Sud, Catania, Italy
[3] Institute of Physics, Jagiellonian University, Kra ków, Poland
[4] Institut für Kern- und Teilchenphysik, Technische Universität Dresden, Dresden, Germany
[5] Joint Institute for Nuclear Research, Dubna, Russia
[6] European Commission, JRC-Geel, Geel, Belgium
[7] Max-Planck-Institut für Kernphysik, Heidelberg, Germany
[8] Dipartimento di Fisica, Università Milano Bicocca, Milan, Italy
[9] INFN Milano Bicocca, Milan, Italy
[10] Dipartimento di Fisica, Università degli Studi di Milano e INFN Milano, Milan, Italy
[11] Institute for Nuclear Research of the Russian Academy of Sciences, Moscow, Russia
[12] Institute for Theoretical and Experimental Physics NRC "Kurchatov Institute", Moscow, Russia
[13] National Research Centre "Kurchatov Institute", Moscow, Russia
[14] Max-Planck-Institut für Physik, Munich, Germany
[15] Physik Department and Excellence Cluster Universe, Technische Universität München, Munich, Germany
[16] Dipartimento di Fisica e Astronomia dell'Università di Padova, Padua, Italy
[17] INFN Padova, Padua, Italy
[18] Physikalisches Institut, Eberhard Karls Universität Tübingen, Tübingen, Germany
[19] Physik Institut der Universität Zürich, Zurich, Switzerland
[20] *Present address*:Department of Physics and Astronomy, University of Pennsylvania, Philadelphia, PA, USA
[21] *Also at*: Moscow Institute of Physics and Technology, Moscow, Russia
[22] *Also at*: International University for Nature, Society and Man "Dubna", Dubna, Russia
[23] *Present address*: LAL, CNRS/IN2P3, Université Paris-Saclay, Orsay, France

Received: 19 May 2016 / Accepted: 12 October 2016 / Published online: 28 November 2016

Abstract Neutrinoless double electron capture is a process that, if detected, would give evidence of lepton number violation and the Majorana nature of neutrinos. A search for neutrinoless double electron capture of ^{36}Ar has been performed with germanium detectors installed in liquid argon using data from Phase I of the GERmanium Detector Array

[a] e-mail: gerda-eb@mpi-hd.mpg.de

(GERDA) experiment at the Gran Sasso Laboratory of INFN, Italy. No signal was observed and an experimental lower limit on the half-life of the radiative neutrinoless double electron capture of ^{36}Ar was established: $T_{1/2} > 3.6 \times 10^{21}$ years at 90% CI.

1 Introduction

The observation of neutrinoless double beta decay ($0\nu\beta\beta$):

$$(A, Z-2) \rightarrow (A, Z) + 2e^{-}, \tag{1}$$

can provide unambiguous information on lepton number violation and indicate the Majorana nature of neutrinos, regardless the physics mechanism responsible for the decay. Currently many experiments are searching for this decay considering different isotopes. Among these there is the GERDA (GERmanium Detector Array) experiment [1] implementing bare germanium detectors enriched in ^{76}Ge. This experiment searches for neutrinoless double beta decay of ^{76}Ge. Recently the best limit on $0\nu\beta\beta$ decay half-life of ^{76}Ge has been published by the GERDA collaboration [2].

Another lepton number violating process that can provide the same information as neutrinoless double beta decay is the double capture of two bound atomic electrons without the emission of neutrinos (0νECEC):

$$2e^{-} + (A, Z+2) \rightarrow (A, Z) + Q, \tag{2}$$

where the quantity Q corresponds to the energy difference between the ground state atoms $(A, Z+2)$ and (A, Z) [3,4].

While in the corresponding process where two neutrinos are emitted (2νECEC) the available energy of the decay is carried away by neutrinos plus X-rays or Auger electrons, in the neutrinoless double electron capture the decay must be accompanied by the emission of at least another particle to ensure energy and momentum conservation. Different modes can be considered in which 0νECEC decay is associated with the emission of different particles like $e^{+}e^{-}$ pairs, one or two photons, or one internal conversion electron. A detailed discussion about double electron capture processes can be found in Refs. [5–7].

For $0^{+} \rightarrow 0^{+}$ transitions the capture of two K-shell electrons with the emission of only one photon is forbidden because of angular momentum conservation. Therefore, the most likely process is the capture from the K- and the L-shell. The diagram of this mode is depicted in Fig. 1. The unstable daughter atom relaxes by emission of X-rays or Auger electrons.

At present, only two experiments found an indication of two neutrino double electron capture. The first is based on a geochemical measurement of ^{130}Ba decay into ^{130}Xe [8,9] and the second is a large-volume copper proportional counter searching for double K-shell capture in ^{78}Kr [10]. Several experiments including the latter established limits on both neutrino accompanied and neutrinoless double electron capture of different isotopes (see Refs. [10–17]). For some isotopes the possibility of a resonant enhancement of the 0νECEC decay has been predicted in case of mass degeneracy between the initial state and an excited final state [4,18].

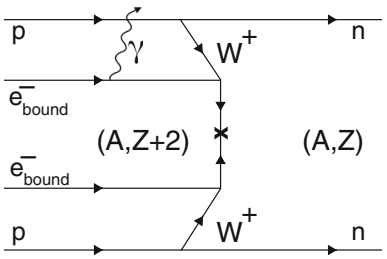

Fig. 1 Diagram for zero neutrino double electron capture with the emission of one photon

^{36}Ar is expected [19] to undergo double electron capture to the ground state of ^{36}S. The available energy [20] of the decay is 432.58 ± 0.19 keV and, therefore, both the radiative and the internal conversion modes are energetically allowed. A resonance enhancement of the decay is not possible for this isotope. Calculations based on the quasiparticle random-phase approximation (QRPA) predict a half-life for ^{36}Ar in the order of 10^{38} years for an effective Majorana neutrino mass of 1 eV [21]. So far, an experimental limit on the radiative mode obtained during detector characterizations in the GERDA Detector Laboratory has been published ($T_{1/2} > 1.9 \times 10^{18}$ years at 68% CL) [22].

The radiative mode of 0νECEC in ^{36}Ar with the emission of one photon provides a clear signature through the discrete value of its energy and allows the detector to be separate from the source of the decay. Two cascades of characteristic X-rays with energies of $E_K = 2.47$ keV and $E_L = 0.23$ keV are emitted [23], corresponding to the capture of the electrons from the K- and the L-shell, respectively. The uncertainties for the energies of the X-rays amount to 0.4 eV. The corresponding energy for the monochromatic photon is $E_\gamma = Q - E_k - E_L = 429.88 \pm 0.19$ keV.

This paper reports the search for the 429.88 keV γ line from 0νECEC decay of ^{36}Ar with GERDA Phase I germanium detectors and the determination of a limit on its half-life.

2 The GERDA experiment

The GERDA experiment [1] is located at the Laboratori Nazionali del Gran Sasso (LNGS) of the INFN. It was

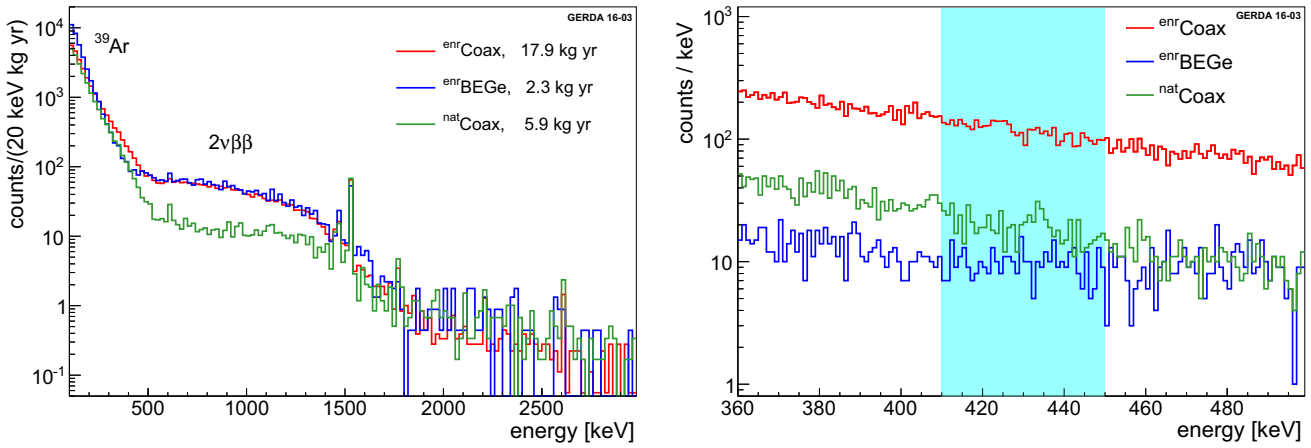

Fig. 2 Energy spectra from the three data sets collected during GERDA Phase I. The *left panel* shows the energy spectra weighted with the product of life time and detector mass. The *right panel* displays the energy region between 360 and 500 keV. The *shaded area* corresponds to the ROI defined between 410 and 450 keV

designed in two phases. During Phase I reprocessed *p*-type semi-coaxial High-Purity Germanium (HPGe) detectors enriched in ^{76}Ge (^{enr}Ge) to up to 86% [24] from the HDM [25] and IGEX [26] experiments have been employed in the experiment as well as natural germanium (^{nat}Ge) HPGe detectors from the GENIUS Test Facility and newly produced enriched Broad Energy Germanium (BEGE) detectors [27]. The bare detectors are immersed into a cryostat containing 64 m^3 (89.2 t) of LAr, which acts both as the coolant medium and a shield against external radiation. The isotopic abundance of ^{36}Ar in natural argon is 0.3336(4)% [28], which sums up to about 298 kg of ^{36}Ar. An additional shield of ultra pure water (10 m in diameter) surrounds the cryostat containing the argon. The water tank is instrumented with 66 PMTs as a muon Cherenkov veto [29]. Each detector string is surrounded by a 60 μm thick Cu foil ("mini-shroud"), to limit drifting of ^{42}K ions to detector surfaces. In addition, to mitigate radon contamination, a 30 μm Cu cylinder ("radon shroud") surrounds the array of strings.

3 Data taking and data selection

The data taking of GERDA Phase I started in November 2011 and ended in May 2013. Until March 2012, the setup included 8 ^{enr}Ge semi-coaxial and 3 ^{nat}Ge semi-coaxial detectors. Two months later, two of the ^{nat}Ge semi-coaxial detectors were replaced by five new ^{enr}Ge BEGE detectors. After this insertion a higher background was observed. Therefore a period of 49 days was excluded from this analysis. The data taking was separated into runs, with a duration of about one month each. Detectors which showed instabilities during specific runs where removed from the analysis. Two detectors showed instabilities from the very beginning of data taking. Therefore, data collected from these detectors were discarded. The total collected data used for the search for 0νECEC of ^{36}Ar correspond to a life time of about 460 d. The data were divided into three different data sets, one containing data from natural semi-coaxial detectors (labeled as ^{nat}Coax), one containing data from enriched semi-coaxial detectors (^{enr}Coax) and the last containing data collected by BEGE detectors (^{enr}BEGe). The energy spectra from the three data sets are shown in Fig. 2. The left panel shows the energy spectra weighted with the product of life time and detector mass. The right panel displays the energy region between 360 and 500 keV. Indeed, in the region around 429.88 keV, enriched and natural detectors are characterized by different contributions to the spectrum, in particular due to $2\nu\beta\beta$ decays from ^{76}Ge in the enriched ones. In addition, BEGE detectors are considered as a separate data set because of the improved energy resolution with respect to semi-coaxial detectors. The main contribution to the spectrum around 430 keV is due to ^{39}Ar β decays. The spectral shape is different for BEGE detectors due to the different detector geometry and outer dead layer thickness.

Offline reconstruction of GERDA data was performed within the GELATIO software framework [30]. Detector signals are read out by charge sensitive preamplifiers and then digitized by 100 MHz flash analog to digital converters (FADCs). Preceded by a ∼80 μs long baseline, the charge signal rises up with a rise time of ∼1 μs and is followed by a ∼80 μs long exponential tail. The energy of each event is estimated by applying an optimized Zero Area Cusp filter [31] to the digitized signal. Cuts based on the baseline slope, the number of triggers and the position of the rising edge were applied to remove pile-up events and accidental coincidences. All detected events within 10 μs from the muon veto trigger were also

rejected. Finally, an anti-coincidence cut was applied to remove events with an energy deposition in more than one detector.

The energy calibration was performed during dedicated calibration runs (every one or two weeks) in which three ^{228}Th sources were lowered to the vicinity of the detectors. In addition, the stability of the system was continuously monitored by injecting test charge pulses into the input of the preamplifiers. The energy dependence of the resolution was obtained for each data set from the summed calibration spectra and then the value at the signal peak position of 429.88 keV was derived. The ^{42}K background γ line at 1524.7 keV in the physics data was used to determine a correction factor in case its energy resolution differed more than one standard deviation from the one obtained during the calibrations. To combine the different values into a single value for the data set, the average of the energy resolution of each detector was calculated weighted with the signal detection efficiency of the detector. The uncertainty on the resolution is primarily coming from the fit of the resolution curve and is largest for the detectors that require the correction factor [32]. The expected Full Width at Half Maximum (FWHM) value at 429.88 keV is 4.08 ± 0.20 keV for the $^{\text{nat}}$Coax, 3.72 ± 0.05 keV for the $^{\text{enr}}$Coax and 2.01 ± 0.10 keV for the $^{\text{enr}}$BEGe data set. The systematic uncertainty on the FWHM, estimated by comparing the resolution of the summed calibration spectra to the average resolution of the single calibrations, is ± 0.05 keV.

4 Determination of the half-life of 0νECEC of ^{36}Ar

A limit on the half-life $T_{1/2}$ of 0νECEC decay of ^{36}Ar was determined considering the data of GERDA Phase I discussed in Sect. 3. The region of interest (ROI) around the signal, the 429.88 keV γ line from the 0νECEC decay, is defined between 410 and 450 keV. The energy spectrum of coincidence events shows the presence of the three γ lines from $^{108\text{m}}$Ag [33]. $^{108\text{m}}$Ag has a half-life of 418 years and undergoes electron capture into the 6^+ excited state of ^{108}Pd with a probability of 91.3%. The de-excitation of the daughter nucleus leads to three equally probable γ rays in the final state, with energies of 433.9, 614.3 and 722.9 keV. The presence of $^{108\text{m}}$Ag was also observed in the screening measurements. For these reasons the 433.9 keV γ line from $^{108\text{m}}$Ag in the ROI was taken into account in the analysis. The determination of the detection efficiency and the analysis result are discussed in the following.

Detection efficiency

The detection efficiency ε is defined as the number of γ rays which entirely deposit their energy inside a single GERDA detector. It has been determined by Monte Carlo simulations employing the MAGE software framework [34] based on GEANT4 [35,36]. 10^9 γ rays with an energy of 429.88 keV were generated in a cylindrical LAr volume with a radius of 67 cm and a height of 130 cm, centered around the detector array. The considered volume corresponds to 1827 l of LAr equivalent to 7.7 kg of ^{36}Ar. A measurement with mass spectrometer showed no difference in the ^{36}Ar abundance between atmospheric and liquid phase within the instrumental sensitivity of 0.5%. The LAr density variation due to temperature differences in the cryostat is less than 1.5% [37]. Within statistical precision both systematic effects are negligible on the limit estimation. The contribution from γ rays originating from outside this volume to the number of full energy depositions is less than the statistical uncertainty of 0.2%. The full efficiency for each data set was derived by summing up the individual detector efficiencies weighted for the life time of each run. Their systematic uncertainty is dominated by two main contributions: the uncertainty on the Monte Carlo processes, whose effect on the efficiency was estimated to be 4%, and the uncertainty on the dead layer of the germanium detectors. The latter was estimated by independently varying for each detector the dead layer values within ± 1 standard deviation. This changes the efficiency of 8–10 % for a single semi-coaxial detector and 3.5–6% for a single BEGE detector. The uncertainty for the three data sets, calculated assuming full correlation among the uncertainties of individual detectors, is 9.2 % for the $^{\text{nat}}$Coax and $^{\text{enr}}$Coax data sets and 4.5 % for the $^{\text{enr}}$BEGe data set. The total systematic uncertainty on the efficiency is obtained by summing in quadrature the two contributions and amounts to 10% for the $^{\text{nat}}$Coax data set, 10% for the $^{\text{enr}}$Coax data set and 6% for the $^{\text{enr}}$BEGe data set.

Statistical uncertainties are negligible with respect to systematic ones. The efficiencies are quoted in Table 1.

Analysis

The expected signal counts S_d from neutrinoless double electron capture from dataset d are related to the half-life $T_{1/2}$ according to the following relation

$$S_d = \ln 2 \cdot \frac{\varepsilon_d}{T_{1/2}} \cdot \frac{N_A \cdot M_{LAr} \cdot f_{36} \cdot t}{m_{Ar}}, \tag{3}$$

where ε_d is the signal detection efficiency for data set d, N_A is the Avogadro constant, t is the total life time, M_{LAr} is the mass of the LAr volume that was used for the efficiency determination, f_{36} the abundance of ^{36}Ar and m_{Ar} the molar mass of argon.

Table 1 Fit parameters values: FWHM is the Full Width at Half Maximum, ε the signal detection efficiency, B_{Ag} the expected number of counts from the 433.9 keV ^{108m}Ag γ line and B_0 the expected number of counts from the linear background component at the signal position

Data set	FWHM (keV)	ε	B_{Ag} (counts)	B_0 (counts/keV)
^{nat}Coax	4.08 ± 0.20	$(2.92 \pm 0.29) \times 10^{-4}$	$41.9^{+14.0}_{-12.9}$	18.3 ± 0.8
^{enr}Coax	3.72 ± 0.05	$(7.06 \pm 0.71) \times 10^{-4}$	$24.6^{+18.6}_{-23.0}$	116.9 ± 1.8
^{enr}BEGe	2.01 ± 0.10	$(1.11 \pm 0.07) \times 10^{-4}$	$0.0^{+5.3}$	9.7 ± 0.6

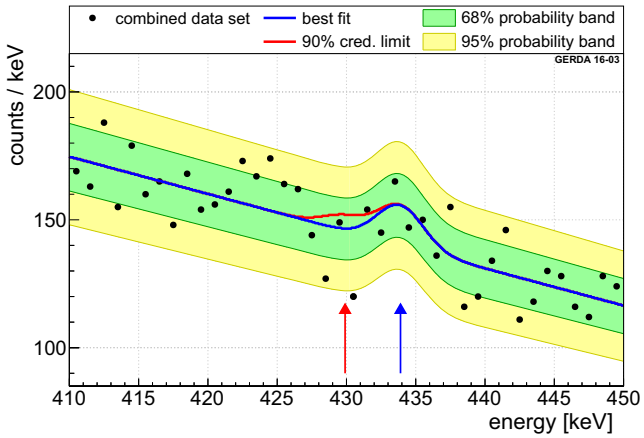

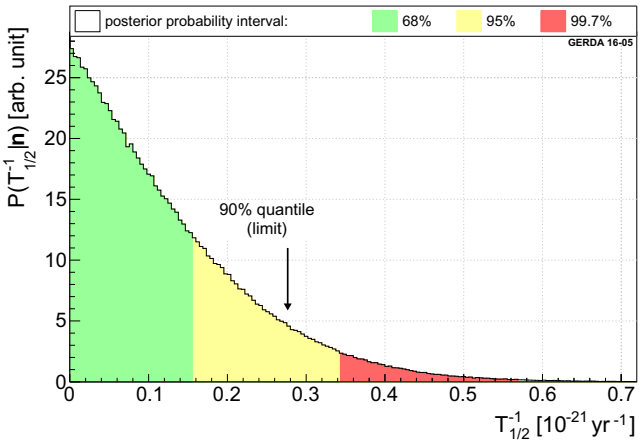

Fig. 3 90% CI Bayesian fit result for the inverse of the half-life on neutrinoless double electron capture of ^{36}Ar. The *left panel* displays the experimental data from GERDA Phase I together with the best fit result (in *blue*) and the 90% credibility interval limit (in *red*). The peak centered at 433.9 keV represents the best fit result for the γ line from ^{108m}Ag. The *arrows* indicate the respective peak positions. The *right panel* shows the marginalized posterior probability distribution for $T^{-1}_{1/2}$, where the *arrow* indicates the 90% quantile from which the limit is derived

The unbinned likelihood function is defined as

$$\mathcal{L} = \prod_d \mu_d^{N_d} e^{-\mu_d} \prod_i^{N_d} \frac{\lambda_{d,i}}{\mu_d}, \tag{4}$$

where the product runs over all data sets d and events i. N_d is the total number of events in the data set. $\lambda_{d,i} = \lambda_d(E_{d,i}|\mathbf{p}_d)$ is the extended probability density of finding an event with energy $E_{d,i}$ in dataset d with a given set of parameters $\mathbf{p}_d$. μ_d represents the total number of expected events in dataset d over the whole energy range $\mu_d = \int \lambda_d(E|\mathbf{p}_d)dE$. In the region of interest the background is in good approximation linear. Therefore, $\lambda_{d,i}$ can be described as the sum of a linear background contribution plus a peak from ^{108m}Ag and the signal peak from 0νECEC of ^{36}Ar

$$\begin{aligned}\lambda_{d,i} = \frac{1}{\sqrt{2\pi}\sigma_d} \Bigg\{ & S_d \cdot \exp\left[-\frac{(E_{d,i} - 429.88 + \delta_E)^2}{2\sigma_d^2} \right] \\ & + B_{\mathrm{Ag,d}} \cdot \exp\left[-\frac{(E_{d,i} - 433.9 + \delta_E)^2}{2\sigma_d^2} \right] \Bigg\} \\ & + B_{0,d} + B_{1,d} \cdot (E_{d,i} - 429.88), \end{aligned} \tag{5}$$

where σ_d is the energy resolution (FWHM $= 2.35 \cdot \sigma_{\mathrm{d}}$), δ_E a possible systematic shift in energy scale. $B_{0,d}$ and $B_{1,d}$ describe the linear background and $B_{\mathrm{Ag,d}}$ the count expectation of the ^{108m}Ag peak. A Bayesian approach was used to extract the posterior probability density on $T^{-1}_{1/2}$. In total, the fit has 17 floating parameters, six describing the signal peak (ε_d, σ_d), six for the linear background ($B_{0,d}$, $B_{1,d}$), three for the ^{108m}Ag peak ($B_{\mathrm{Ag,d}}$). $T^{-1}_{1/2}$ and δ_E are in common to all data sets. The parameters ε_d, σ_d and δ_E are constrained by Gaussian shaped prior distributions whose standard deviation is given by their systematic uncertainty. A flat prior is considered for the remaining parameters, including the inverse half-life $T^{-1}_{1/2}$. Furthermore, $B_{0,d}$, $B_{Ag,d}$ and $T^{-1}_{1/2}$ are bound to positive values, while $B_{1,d}$ is bound to negative values. The best fit is defined as the mode of the global posterior probability density and yields $T^{-1}_{1/2} = 0$, i.e. no signal events from 0νECEC. The 90% credibility limit of the half-life, defined as the 90% quantile of the marginalized posterior distribution, is

$$T_{1/2} > 3.6 \cdot 10^{21} \mathrm{yr}\ (90\%\mathrm{CI}). \tag{6}$$

The median sensitivity for the 90% CI limit was estimated with toy Monte Carlo simulations and is equal to $2.7 \cdot$

10^{21} years. The sum spectrum of all data sets around the ROI and the fit functions are displayed in Fig. 3 together with the marginalized posterior distribution for $T_{1/2}^{-1}$.

Systematic uncertainties are directly folded into the fit through the Gaussian priors associated to parameters ε_d, σ_d and δ_E. They weaken the limit by about 0.3%, which was evaluated by fixing these 7 parameters and repeating the fit with the remaining 10 parameters. To test if the model described in Eq. 5 is sufficient, the p value was calculated for the three data sets, as proposed in Ref. [38] using a 1 keV binning. The obtained values are 0.96, 0.11 and 0.91 for the $^{\text{nat}}$Coax, $^{\text{enr}}$Coax and $^{\text{enr}}$BEGe data sets respectively and indicate that the model describes the data sufficiently well. The fit result for B_{Ag} shows the presence of the 433.9 keV γ line in the $^{\text{nat}}$Coax data set. The 90% CI limit is reduced by 10 % in case the presence of this line is neglected in the fit. The expectation value for the number of counts from the $^{108\text{m}}$Ag γ line for the three data sets is reported in Table 1 together with the fit result for B_0 which represents the number of events from the linear background component at the signal peak energy of 429.88 keV (third term of Eq. 5). In the same table the efficiency values and the energy resolution are also reported.

5 Conclusions

GERDA established the most stringent half-life limit on the radiative mode of neutrinoless double electron capture of ^{36}Ar with Phase I data. The limit is three orders of magnitude better than previous results for this isotope; however, it is still orders of magnitude far from the theoretical prediction from QRPA calculations.

Acknowledgements The GERDA experiment is supported financially by the German Federal Ministry for Education and Research (BMBF), the German Research Foundation (DFG) via the Excellence Cluster Universe, the Italian Istituto Nazionale di Fisica Nucleare (INFN), the Max Planck Society (MPG), the Polish National Science Centre (NCN), the Foundation for Polish Science (MPD programme), the Russian Foundation for Basic Research (RFBR), and the Swiss National Science Foundation (SNF). The institutions acknowledge also internal financial support. The GERDA collaboration is grateful for useful discussions with V. Tretyak. The GERDA collaboration thanks the director and the staff of LNGS for their continuous strong support of the GERDA experiment. Furthermore we acknowledge the use of the CPU farm ATLAS of ZIH at TU Dresden for the Monte Carlo simulations.

Funded by SCOAP^3.

References

1. K.-H. Ackermann et al. (Gerda collaboration), Eur. Phys. J. C **73**, 2330 (2013)
2. M. Agostini et al. (Gerda collaboration), Phys. Rev. Lett. **111**, 122503 (2013)
3. R.G. Winter, Phys. Rev. **100**, 142 (1955)
4. J. Bernabeu et al., Nucl. Phys. B **223**, 15 (1983)
5. V. Vergados, Nucl. Phys. B **218**, 109 (1983)
6. M. Doi, T. Kotani, Prog. Theor. Phys. **89**, 129 (1993)
7. F. Simkovic et al., Prog. Part. Nucl. Phys. **66**, 446 (2011)
8. A.P. Meshik et al., Phys. Rev. C **64**, 035205 (2001)
9. M. Pujol et al., Geochim. Cosmochim. Acta **73**, 6834 (2009)
10. Y.M. Gavrilyuk et al., Phys. Atom. Nucl. **78**, 13 (2015)
11. Ch. Briançon et al. (TGV-2 collaboration). Phys. Atom. Nucl. **78**, 740 (2015)
12. D.M. Mei et al., Phys. Rev. C **89**, 014608 (2014)
13. M. Jeskovsky et al., Nucl. Instrum. Methods A **795**, 268 (2015)
14. P. Belli et al., Phys. Rev. C **93**, 045502 (2016)
15. P.P. Povinec et al., AIP Conf. Proc., vol. 1686 (2015), p. 020018
16. A.S. Barabash et al., Nucl. Phys. A **807**, 269 (2008)
17. A.S. Barabash et al., Phys. Rev. C **83**, 045503 (2011)
18. S. Eliseev et al., Phys. Rev. Lett. **106**, 052504 (2011)
19. V.I. Tretyak, YuG Zdesenko, At. Data Nucl. Data Tables **80**, 83 (2002)
20. M. Wang et al., Chin. Phys. C **36**, 1636 (2012)
21. A. Merle, Ph.D. Thesis, University of Heidelberg (2009)
22. O. Chkvorets, Ph.D. Thesis, University of Heidelberg (2008). arXiv:0812.1206
23. G.P. Williams, in *X ray data booklet*, ed. by A.C. Thompson et al. Electron Binding Energies (2009). http://xdb.lbl.gov/Section1/Table1-1a.htm
24. M. Agostini et al. (Gerda collaboration), Eur. Phys. J. C **75**, 39 (2015)
25. M. Günther et al., Phys. Rev. D **55**, 54 (1997)
26. A. Morales, Nucl. Phys. B **77**, 335 (1999)
27. Canberra Semiconductor NV., Lammerdries-Oost 25, B-2439 Olen, Belgium
28. J.-Y. Lee et al., Geochim. Cosmochim. Acta **70**, 17 (2006)
29. K. Freund et al., Eur. Phys. J. C **76**, 298 (2016)
30. M. Agostini et al., J. Instrum. **6**, P08013 (2011)
31. M. Agostini et al. (Gerda collaboration), Eur. Phys. J. C **75**, 255 (2015)
32. G. Benato, Ph.D. Thesis, University of Zürich (2016)
33. M. Agostini et al. (Gerda collaboration), J. Phys. G Nucl. Part. Phys. **42**, 115201 (2015)
34. M. Boswell et al., IEEE Trans. Nucl. Sci. **58**, 1212 (2011)
35. S. Agostinelli et al., (Geant collaboration), Nucl. Inst. Meth. A **506**, 250 (2003)
36. J. Allison et al., IEEE Trans. Nucl. Sci. **53**, 270 (2006)
37. Ch. Haberstroh, A.I.P. Conf, Proc. vol. 985 (2008), p. 1201
38. F. Beaujean, A. Caldwell, J. Stat. Plan. Inference **141**, 11 (2011)